Available online at www.sciencedirect.com
SCIENCE DIRECT
Polymer 46 (2005) 4330–4343
polymer
www.elsevier.com/locate/polymer

The atomistic simulation of the gas permeability of poly(organophosphazenes). Part 2. Poly[bis(2,2,2-trifluoroethoxy)phosphazene]

N. Hu, J.R. Fried*

Department of Chemical and Materials Engineering, Polymer Research Center, OBR Center for Computer-Aided Molecular Design, University of Cincinnati, Cincinnati, OH 45221-0012, USA

Available online 18 April 2005

Abstract

Self-diffusion and sorption of seven gases (He, H_2, O_2, N_2, CH_4, CO_2, and Xe) in poly[bis(2,2,2-trifluoroethoxy)phosphazene] (PTFEP) have been investigated by molecular dynamics and Grand Canonical Monte Carlo (GCMC) simulations of two amorphous cells and an α-orthorhombic crystalline supercell. In the case of MD simulation of diffusion coefficients, values obtained for both amorphous and crystalline PTFEP are similar and comparable to experimental values reported for semicrystalline samples. These results indicate that gas diffusion is unrestricted in the crystalline state of PTFEP as has been reported for poly(4-methyl-1-pentene) (PMP) and, more recently, for a crystalline form of syndiotactic polystyrene (sPS).

In contrast to both PMP and sPS that have low-density crystalline forms, only He exhibits any solubility in the α-orthorhombic crystalline cells of PTFEP during simulation. In addition, values of the solubility coefficients obtained from simulation of the amorphous cells are three to five times larger than would be expected by extrapolating values reported for semicrystalline samples to 100% amorphous content. These results suggest that while the crystalline domains do not restrict gas diffusivity in PTFEP, they significantly reduce gas solubility in semicrystalline PTFEP through the reduction of amorphous content and through some additional effect of the crystallites on amorphous-phase solubility, possibly through chain immobilization of the amorphous phase. Similar solubility behavior has been suggested for polyethylene on the basis of recent simulation studies.

As reported in a prior communication, the solubility of CO_2 in PTFEP is very high compared to other gases due to a weak quadrupole–dipole interaction between CO_2 and the trifluoroethoxy group of PTFEP. As a result, the solubility coefficients of CO_2 obtained from GCMC simulation of the amorphous cells and from permeability measurements of semicrystalline samples are both larger than predicted by a simple correlation of gas solubility coefficients with the Lennard-Jones potential well parameter, ε/k, of other gases as proposed by Teplyakov and others. A modified form of this correlation that includes a Flory interaction term is shown to fit all gas solubility data for this polymer including that of CO_2.

Keywords: Poly[bis(2,2,2-trifluoroethoxy)phosphazene]; CO_2 solubility; Gas diffusivity

1. Introduction

The previous communication [1] reported results of the atomistic simulation of diffusion (NVT-dynamics) and gas solubility (Grand Canonical Monte Carlo, GCMC) of six gas molecules (He, Ne, O_2, N_2, CH_4, and CO_2) in two isomeric forms of poly(dibutoxyphosphazenes)—poly-[bis(*n*-butoxy)phosphazene] (PnBuP) and poly[bis(*sec*-butoxy)phosphazene) (PsBuP). The force field used in these studies was COMPASS (condensed-phase optimized molecular potentials for atomistic simulation studies) [2]. COMPASS is a class II, ab initio force field that has been extensively parameterized and validated for alkanes and benzene compounds [2], for many inorganic molecules and gases [3], for aliphatic azide compounds [4], as well as for polyorganophosphazenes [1,5,6]. In general, simulation results obtained in the previous study agreed reasonably well with experimental values reported by Hirose et al. [7] for the diffusion coefficients (D) of gases in PnBuP and PsBuP and for the solubility coefficient (S) of gases in PnBuP. In the case of PsBuP, solubility coefficients

* Corresponding author.

0032-3861/$ - see front matter © 2005 Elsevier Ltd. All rights reserved.
doi:10.1016/j.polymer.2005.03.017

obtained by GCMC simulation of an amorphous cell were significantly larger than the reported effective solubility coefficients (i.e. $S=P/D$). It was suggested in the previous study, that the sample of PsBuP used by Hirose et al. [7] may not have been totally amorphous. Evaluation of chain flexibility by means of vectorial autocorrelation function (VACF) analysis of these two poly(dibutoxyphosphazenes) and also that of poly[bis(*iso*-butoxy)phosphazene] (PiBuP) indicated that diffusion coefficients increased while diffusive selectivity to molecules of different sizes (i.e. D(He)/D(CH_4)) decreased with increasing mobility of the polymer chain.

While long-chain alkoxy-substituted poly(organophosphazenes) such as PnBuP are amorphous, many polyphosphazenes are semicrystalline and exhibit two first-order transitions [8–10]. The lower temperature transition corresponds to a phase change, $T(1)$, from a crystalline structure ordered in three directions to a mesophase with a loss in lateral ordering. The most extensively studied member of these polyphosphazenes is poly[bis(2,2,2-trifluoroethoxy) phosphazene] (PTFEP) [11]

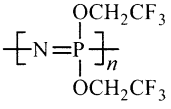

whose crystalline morphology [12–16] and gas transport properties [7,17–19] have been widely reported. PTFEP has three polymorphic crystalline forms—a monoclinic β-modification and orthorhombic α- and γ-modifications [15]. The orthorhombic α-modification incorporates two monomer units per unit cell while the γ-modification contains four monomer units [15,20]. PTFEP has a glass transition temperature near 207 K, undergoes the $T(1)$ transition to a hexatic (smectic) [10] mesophase (δ-form) [15] between 343 and 363 K [8], and displays a crystalline melting temperature in the vicinity of 513 K [21,22]. In an earlier communication, Fried and Ren [6] reported excellent representation of the glass transition of PTFEP using NPT dynamics and the COMPASS force field. In a subsequent publication [23], results of a simulation study of the mesophase transition in PTFEP will be reported.

Representative gas permeabilities and permselectivities reported for PTFEP are compared with those reported for PnBuP, PiBuP, and PsBuP in Table 1. Although less permeable than the polybutoxyphosphazenes for most gases, PTFEP has potential as a high-temperature membrane for both O_2 [18] and CO_2 [19] separation due to its high thermal stability ($T_m \sim 513$ K). Of particular note, PTFEP displays an attractive combination of both high permeability and high permselectivity for CO_2 (over methane) due to high CO_2 solubility as shown in Table 1. In a study by Hirose et al. [7], the solubility of CO_2 (as well as N_2O) was shown to be significantly higher than would be expected on the basis of the commonly used correlation that relates the gas solubility coefficient (S) with the Lennard-Jones potential-well depth, ε/k, a measure of gas condensability, in the form [24]

$$\log S = \log S^0 + m\left(\frac{\varepsilon}{k}\right) \tag{1}$$

where S^0 is a constant. As an approximation, the slope m is independent of the polymer and is in the order of 10^{-2} K^{-1}. Results similar to those of Hirose et al. [7] showing elevated CO_2 solubility have been reported by Starannikova et al. [19] in a study of five gases (Xe, O_2, N_2, CO_2, and CH_4) in two samples of PTFEP having different crystallinity. Experimental solubility data reported by Hirose et al. is plotted as a function of ε/k in Fig. 1. Also shown for comparison are the corresponding plots of experimental solubility for PnBuP, PsBuP, and PiBuP [25] that show that CO_2 solubility for these polyphosphazenes, unlike that of PTFEP, follows the correlation of Eq. (1) as is typical for most polymers.

Teplyakov and Meares [26] have proposed a relationship equivalent to that of Eq. (1) but expressed in the more generalized form

$$\log S = K_3 - K_4\left(\frac{\varepsilon}{k}\right) \tag{2}$$

where the parameters K_3 and K_4 are polymer-specific. In the previous communication [1], Eq. (2) was shown to provide good correlation of both experimental [25] and GCMC simulation data for all gases including CO_2 in PnBuP and in PsBuP. It was noted in the previous study that simulation values of the solubility coefficients in amorphous PsBuP were consistently higher than reported experimental values. A reason offered for this discrepancy was the possibility that

Table 1
Permeabilities and permselectivities of selected polyphosphazenes

	f[a]	$P(O_2)$[b]	$P(O_2)/P(N_2)$	$P(CO_2)$[b]	$P(CO_2)/P(CH_4)$
PnBuP[c]	0.097	128	2.29	647	3.30
PiBuP[c]	0.091	86.6	2.73	395	4.00
PsBuP[c]	0.084	40.7	3.04	177	4.53
PTFEP[d]	0.154	35.4	2.41	196	10.3

[a] Fractional free volume obtained by the transition-state method of Suter and Gusev [63,75].
[b] Units of barrer, 10^{-10} cm^3 (STP)-cm/(cm^2 s cm Hg).
[c] Permeability data of Hirose and Mizoguchi [25]; fractional free volume reported by Fried and Ren [1].
[d] Permeability data of Hirose et al. [7]; fractional free volume of 150-r.u. amorphous cell, this study.

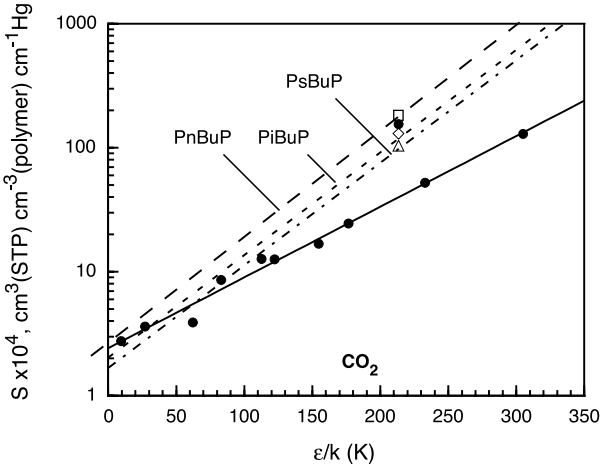

Fig. 1. Semilogarithmic plot of experimental solubility coefficients, S, versus the Lennard–Jones potential well-depth parameter, ε/k, following the correlation given by Eq. (1). The solid line represents the least-squares fit of the data of Hirose et al. [7] for PTFEP (60% crystallinity) (•) with the exclusion of the solubility coefficient for CO_2. Least-squares fits (dotted lines) of experimental data [25] for PnBuP (△), PiBuP (◇), and PsBuP are shown for comparison. Only CO_2 data points are shown for PnBuP (□), PiBuP (ε) and PsBuP (ν). The vertical broken line identifies the location of the Lennard–Jones potential well-depth parameter, ε/k, (213.4 K) for CO_2.

the sample of PsBuP used in that study may have not been totally amorphous.

The high solubility of CO_2 in PTFEP has been attributed to an interaction between CO_2 and the electron-withdrawing trifluoroethoxy groups of PTFEP [7,19]. Carbon dioxide, which does not have a permanent dipole moment, does have a large quadrupole moment [27]. Similar enhancement of CO_2 solubility has been reported for other fluorinated polymers such as poly(trifluoropropyl methyl siloxane) (PTFPMS) [17,28,29], fluorine-containing polycarbonates [30], poly(vinylidene fluoride) [31,32], poly[*o*-(trifluoromethyl)phenylacetylene] [33], and poly[5,5-difluoro-6,6-bis(trifluoromethyl)norbornene] [34]. Stern [29] has speculated that the high solubility of CO_2 in PTFPMS may be a result of a specific interaction between CO_2 and the polar trifluoropropyl group. In a recent ab initio study of the interaction of CO_2 with low-molecular-weight fluorinated alkanes, we have shown that the high CO_2 permeability of PTFEP may be attributed to a weak dipole–quadrupole interaction between the trifluoroethoxy groups of PTFEP and CO_2 [35]. This was confirmed in that study by MD simulation using pair correlation function analysis of the association of CO_2 with the trifluoroethoxy groups.

As noted above, an important difference between PTFEP and PnBuP is that PTFEP is a microcrystalline polymer with several crystal forms and a first-order mesophase transition, $T(1)$. Gas transport above $T(1)$ has been studied by Mizoguchi et al. [17] who reported that gas solubility in the mesophase is only about 55–70% of that in the amorphous phase while the diffusion coefficient in the mesophase is almost the same as in the amorphous phase. Assuming that gas solubility in the crystalline phase was negligible, Mizoguchi et al. [17] had proposed that solubility below $T(1)$ could be represented as

$$S_1 = X_a S_a \tag{3}$$

where X_a is the amorphous fraction (at the measurement temperature) and S_a is the solubility of the amorphous phase, respectively. The solubility above $T(1)$ was represented as

$$S_2 = X_a S_a + (1 - X_a) S_m \tag{4}$$

where S_m is the (reduced) solubility of the gas in the mesophase. For CO_2, S_a and S_m at 75 °C were estimated to be 0.0161 and 0.0108 cm^3 (STP) cm^{-3} $cm\,Hg^{-1}$, respectively.

As previously mentioned, Mizoguchi et al. [17] suggested that gas diffusivity is negligible in the crystalline phase of PTFEP as commonly assumed for semicrystalline polymers. In contrast, Starannikova et al. [19] have measured the gas permeability of PTFEP at 25 and 90 °C for two samples of different crystallinity and concluded that the α- and γ-crystalline forms are gas permeable as has been reported to be the case for poly(4-methyl-1-pentene) (PMP) [36,37], a semicrystalline polymer with a crystalline density ($\rho_{crys} = 0.830$ g cm^{-3}) that is slightly lower than that of the amorphous phase ($\rho_{amorph} = 0.838$ g cm^{-3}) [38]. The low density of the crystalline phase of PMP has been attributed to loose packing of the 7/2 helix of PMP in the crystalline state [38]. The solubilities of CO_2 and CH_4 in the crystalline phase of PMP were estimated to be about 25–30% of the solubility of the amorphous phase while gas diffusion in the crystalline phase was only moderately reduced. Another recent example of a polymer that has an open crystalline form is syndiotactic polystyrene (sPS) that can clathate a variety of penetrants to form a complex in its crystalline δ-form [37,39–42]. The density of the δ-form is significantly lower than amorphous sPS [42] due to the loose packing of its helical chains.

The permeability characteristics of semicrystalline PTFEP, PMP, and sPS differ from the usual behavior of semicrystalline polymers for which sorption and diffusion of gases occur exclusively in the amorphous regions while the crystalline domains are non-sorbing and non-permeable due to tighter packing of the ordered crystalline phase [43]. In 1961, Michaels and Bixler [44] proposed that the diffusion coefficient of a gas in the amorphous phase of a semicrystalline polymer is reduced by two separate effects of the crystallites. One is the increased tortuosity of the path that a diffusing molecule must follow due to physical presence of the impervious crystallites and the other is a reduction in the mobility of the amorphous-phase polymer chains. Quantitatively, these effects on diffusion were modeled by introducing a tortuosity factor, τ (a function of amorphous content as well as crystalline morphology) and a chain immobilization factor, β, a measure of restricted segmental mobility near the interface. The form of the equation was

given as

$$D = \frac{D^*}{\tau\beta} \tag{5}$$

where D^* is the diffusion coefficient for the gas in the amorphous polymer. Both D^* and β are functions of the molecular diameter of the gas molecule. In this model [44], gas solubility was given by the simple two-phase model of Eq. (3) in the form

$$S = \alpha S^* \tag{6}$$

where α is the amorphous fraction of the amorphous phase and S^* is the solubility coefficient for the amorphous polymer. Support for the immobilization model has been given recently by Mogri and Paul [45] in a study of gas permeability of a side-chain crystalline polymer. In another study, Budzien et al. [46] have suggested that the presence of crystallites affects the nature of the amorphous phase and influences not only diffusivity in the amorphous phase but also solubility to a larger extent than predicted by this simple model.

It is noted that the conclusion of Starannikova et al. [19] concerning the permeability of the crystalline forms of PTFEP differs from that of Mizoguchi et al. [17] who suggest that the crystalline phase of PTFEP is impermeable. Starannikova et al. had reported that the diffusion coefficients at 25 °C (i.e. below $T(1)$) are nearly independent of crystallinity while solubility is lower for the more crystalline sample. These observations may be attributed to the fact that the density of the crystalline phase (1.73–1.78 g cm^{-3}) is believed to be close to that of the amorphous phase (the density of semicrystalline PTFEP is 1.71 g cm^{-3}). This belief is supported by our earlier simulation study of the glass transition of polyphosphazenes [6], in which NPT dynamics (COMPASS force field) yielded a density of 1.6330 ± 0.0375 g cm^{-3} for amorphous PTFEP. The current study seeks to explore the nature of gas diffusion and solubility in both amorphous and crystalline PTFEP through means of molecular simulations using the COMPASS force field. To our knowledge, the only other MD investigation of gas diffusion in a crystalline polymer has been the study of Müller-Plathe [47] who showed that CO_2 and CH_4 diffuse freely through a tetragonal unit cell of PMP. In the case of CO_2, diffusion was approximately 50% higher parallel to the helical direction than perpendicular to it. By comparison, diffusion of spherically-shaped CH_4 was nearly isotropic. Use of the Widom [48,49] test-particle insertion method indicated that CO_2 and CH_4 solubility in the crystalline unit cell of PMP was reduced but not negligible. Similar results were reported by Zanuy et al. [50] using the AMBER force field and the Widom method to determine solubility.

2. Computational methodology

2.1. Construction of the PTFEP amorphous cell

Single chains of PTFEP having either 120 and 150 repeat units (r.u.) were built using the polymerizer module of Insight II (Accelrys, version 4.0.0 P). For calculations of electrostatic interactions by the charge-group method, the neutral charge groups of the PTFEP repeat unit were assigned to $NP(OCH_2)_2$ and CF_3. The conformational energy of the polymer chain was then minimized for 1000 steps using the COMPASS force field without a non-bond cut-off. The resulting polymer chain was used to construct periodic amorphous cells by means of the amorphous_cell module of Insight II. Five different cells were constructed from both the 120- and 150-r.u. chains. A 100-step minimization process was used to refine the resulting cells. This was followed by an annealing procedure described in the previous communication [1]. Two periods of NPT dynamics (50 and 100 ps) were followed by 50-ps NVT dynamics to further equilibrate the polymer structures. For both the 120- and 150-r.u. structures, the cell having the smallest energy and density variation during the final 100-ps NPT dynamics run was selected from five cells for the simulation of gas diffusivity and solubility. The length of each side of the selected 150-r.u. cell was 32.9 Å. Density obtained from 200-ps NPT dynamics was 1.69 g cm^{-3}. The 120-r.u. amorphous cell was slightly smaller (i.e. 30.9 Å on a side); density was 1.66 g cm^{-3}. These values are in good agreement with the previously reported density [6] of 1.6330 ± 0.0375 obtained from NPT dynamics of amorphous PTFEP at 298 K as illustrated in Fig. 2. As reported earlier [6] and further illustrated in Fig. 2, excellent agreement was obtained between the experimental and simulated densities of the three polybutoxyphosphazenes. These results provide additional validation of the COMPASS force field for polyphosphazenes.

2.2. Construction of PTFEP crystalline cells

Two PTFEP monomeric units with a planar *cis–trans* identity period of 4.9 Å were used to construct an α-orthorhombic unit cell using the solid builder of Insight II (Accelrys). Complete details of the building procedure have been given elsewhere [51]. The cell density and energy were determined after 200-ps NPT dynamics following 2-ps NVT dynamics. The Andersen method [52] was used for temperature control and the Berendsen method [53] for pressure control during NPT dynamics. For solubility calculations using the Widom particle insertion method, two unit cells were linked in the z-direction (i.e. the chain direction) as done by Müller-Plathe [47] for PMP. Resulting dimensions were $a = 10.32$ Å, $b = 9.56$ Å, and $c = 9.81$ Å. For simulation of both diffusivity and solubility, a supercell of the α-modification of PTFEP was built by overlaying four periodical unit cells in the a- and b-direction, respectively,

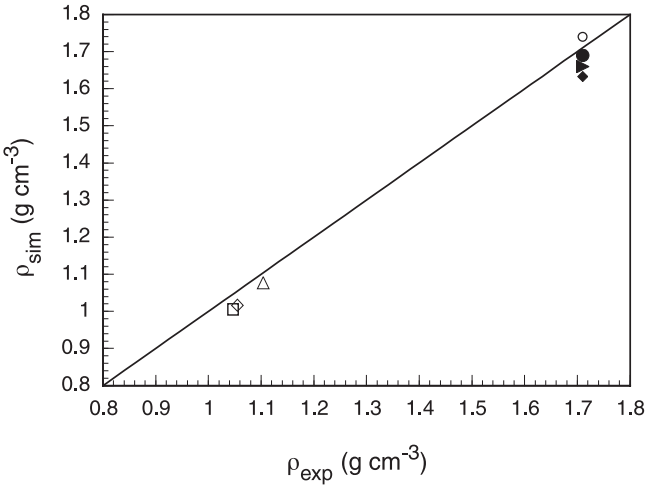

Fig. 2. Plot of densities obtained from simulation (NPT dynamics at 298 K) versus reported experimental values. Simulation values: (□), PnBuP (50-r.u. amorphous cell, Fried and Ren [6]); (◇) PiBuP (50-r.u. amorphous cell, Fried and Ren [6]); (△) PsBuP (50-r.u. amorphous cell, Fried and Ren [6]; (♦) PTFEP, (50-r.u. amorphous cells (Fried and Ren [6]); (▶) PTFEP (120-r.u. amorphous cell, this study); (•) PTFEP (150-r.u. amorphous cell, this study) (○) PTFEP, α-orthorhombic supercell (this study). Experimental densities used for PnBuP, PiBuP, and PsBuP were taken from Hirose and Mizoguichi [25]; the density (1.707 g cm^{-3}) used for PTFEP (60% crystallinity) was reported by Hirose et al. [7].

and eight unit cell images in the chain direction (*c*-direction). The resulting supercell, approximately 38 Å in length, was equilibrated using 1000 minimization steps, 5-ps NVT dynamics, and a final 20-ps NPT dynamics employing a 12-Å cut-off and spline width of 1.0 Å. The dimensions of the resulting orthorhombic supercell, shown in Fig. 3, were $a=40.56$ Å, $b=38.58$ Å, and $c=37.4$ Å. The density obtained from a 200-ps NPT dynamics of the supercell was 1.74 g cm^{-3} at 298 K. This is only 3% larger than the density (1.69 g cm^{-3}) obtained for the larger of the two amorphous cells and is close to the value of 1.707 g cm^{-3} reported for a 60% crystalline sample [7] as shown in Fig. 2.

2.3. Simulation of gas diffusion

Self-diffusion coefficients for seven gases (H_2, He, CH_4, N_2, O_2, CO_2, and Xe) in PTFEP were obtained at 298 K from NVT dynamics. In each case, four gas molecules of a single gas were inserted in the crystalline PTFEP supercell and in the amorphous cells in such a way that the distance between any two gas molecules was at least half the cell length. A period of 2-ns NVT-dynamics, the Andersen thermostat [52], and a 12-Å cut-off were used to obtain self-diffusion coefficients. From trajectories recorded at 1-ps intervals during NVT dynamics, mean-square displacement (MSD) data were obtained and exported to a MatLab program (Mathworks, MA) that used a least-squares algorithm to search for the Einstein diffusion regime from the averaged MSD of four molecules. The Einstein

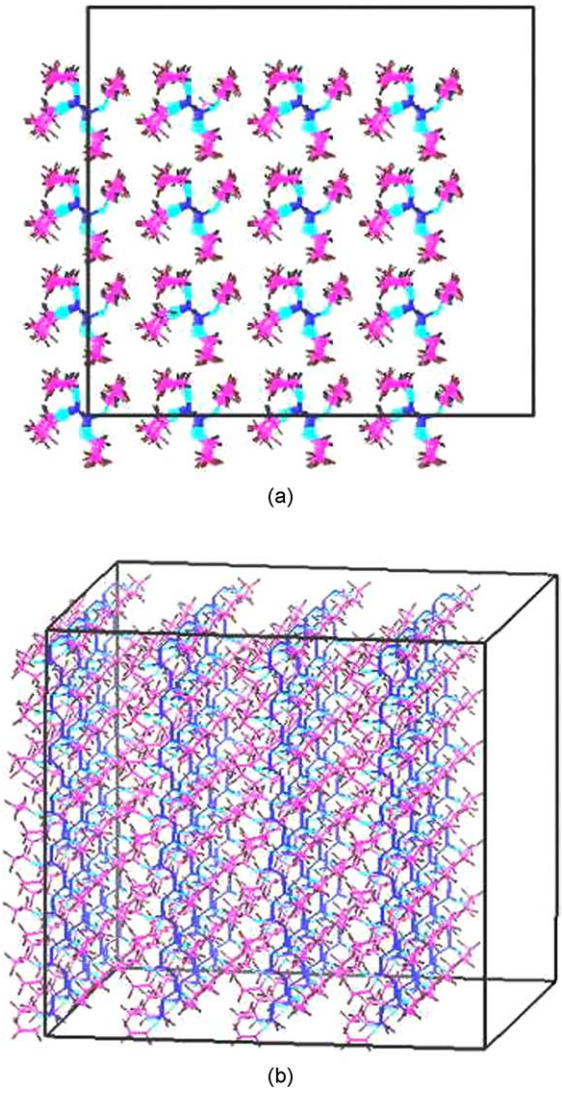

Fig. 3. Top (a) and side (b) views of the α-orthorhombic supercell (41×37×39 $Å^3$) equilibrated at 298 K.

relationship assumes a random walk for the diffusing species. For slow diffusing species, anomalous diffusion is sometimes observed and is characterized by

$$\langle|\mathbf{r}_i(t)-\mathbf{r}_i(0)|\rangle \propto t^n \tag{7}$$

where $n<1$ ($n=1$ for Einstein diffusion regime). At sufficiently long time (i.e. the hydrodynamic limit), a transition from anomalous to Einstein diffusion ($n=1$) may be observed. From the selected MSD data, the self-diffusion coefficient, D_α, was obtained from the MSD of one gas molecule by means of the Einstein equation in the form [54]

$$D_\alpha = \frac{1}{6N_\alpha}\lim_{t\to\infty}\frac{\mathrm{d}}{\mathrm{d}t}\sum_{i=1}^{N}\langle|\mathbf{r}_i(t)-\mathbf{r}_i(0)|^2\rangle \tag{8}$$

In Eq. (8), N_α is the number of diffusing atoms α (i.e. oxygen atoms in O_2), $\mathbf{r}_i(0)$ and $\mathbf{r}_i(t)$ are the initial and final positions of the center of mass of one gas molecule *i* over

the time interval t, and $\langle|\mathbf{r}_i(t) - \mathbf{r}_i(0)|^2\rangle$ is the MSD averaged over the ensemble.

2.4. Determination of chain flexibility

A segmental vectorial autocorrelation function (VACF) [1,55] was used to investigate both main-chain and side-chain flexibility. By defining a vector, $\mathbf{u}(t_0)$, that represents the orientation of a chain segment (backbone or side chain) at a given time, t_0, the angle by which the orientation changes over time, t, is given as [56]

$$m(t) = \langle \mathbf{u}(t_0)\mathbf{u}(t_0 + t)\rangle \tag{9}$$

Ensemble averages were computed over 200 ps of NPT dynamics. In the case of PTFEP, a main-chain vector was chosen as extending from $P(i)$ to $N(i+1)$ in the sequence $–P(i)–N(i)–P(i+1)–N(i+1)–$. For the side chain, the vector was chosen to extend from $P(i)$ to the terminal carbon atom of a trifluoroethoxy CF_3 group attached to $P(i)$ (i.e. $P(i)$–O–C–C).

2.5. Simulation of gas sorption

Solubility coefficients of the seven gases (H_2, He, CH_4, N_2, O_2, CO_2, and Xe) in PTFEP at 298 K were obtained by using the Grand Canonical Monte Carlo (GCMC) method implemented in the sorption module of Insight II (Accelrys). This procedure uses a Metropolis [57] algorithm for accepting or rejecting configurational moves (rotation and translation of the sorbate molecules) as well as for sorbate insertion and deletion. A cut-off distance of 12 Å was used in the simulation and pressure was increased from 0.05 to 0.5 kPa at intervals of 0.05 kPa. For gases with large solubility, (e.g. Xe and CO_2), a lower pressure region (i.e. 0.01 to 0.1 kPa) was used. At each pressure, a total of 500,000 GCMC steps were used. The resulting isotherms were used to calculate the gas solubility coefficient from the limiting slope of the sorption isotherm as described in the previous communication [1].

For comparison in selected cases, solubility coefficients were calculated by the Widom particle-insertion method [48,49] as

$$S = \exp\left(-\frac{\mu_{ex}}{RT}\right) \tag{10}$$

The excess chemical potential of the dissolved gas molecules, μ_{ex}, appearing in Eq. (10) is calculated from the equation

$$\mu_{ex} = -kT \ln\langle \exp\left(-\frac{E}{kT}\right)\rangle \tag{11}$$

where E is the energy of interaction energy of a gas molecule with the polymer and k is the Boltzmann constant. Brackets denote an ensemble average. For both amorphous and crystalline cells, a total of 200,000 iteration steps were used.

3. Results and discussion

3.1. Gas diffusion

The logarithmic values of experimental diffusion coefficients obtained from time-lag measurements for eleven gases and small hydrocarbons in PTFEP (60% crystallinity) [7] are plotted versus the square of the effective diameter, d_{eff}, of the diffusing species in Fig. 4. A least-squares line was fitted to all the data. The plot follows the form of the correlation of Teplyakov and Meares [26] for diffusion coefficients

$$\log D = K_1 - K_2 d_{eff}^2 \tag{12}$$

where the parameters K_1 and K_2 are polymer dependent. Effective diameters used for the plot in Fig. 4 are those tabulated by Teplyakov and Meares from a comparison of the diffusion coefficients of various gases with those for inert gases in different polymers [58]. With the exception of Ne which may be anomalous, all experimental values fall near the correlation line obtained by a least-squares fit of experimental data obtained by Hirose et al. [7] for semicrystalline PTFEP (60% crystallinity). For comparison, the corresponding least-squares lines for the experimental diffusion coefficients for the three polybutoxyphosphazenes have been included in Fig. 4. The comparison shows that diffusion in semicrystalline PTFEP is very comparable to that reported for PsBuP. Both PTFEP and PsBuP exhibit high selectivity to molecules of varying sizes compared to PiBuP and particularly PnBuP. Results of the previous molecular simulation study [1] of PnBuP and PsBuP had

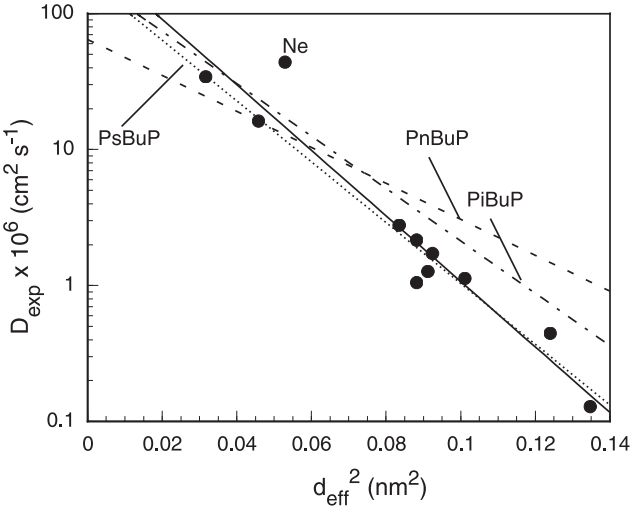

Fig. 4. Plot of experimental diffusion coefficients (D_{exp}) against the square of the effective gas diameters, d_{eff}, as tabulated by Teplyakov and Meares [26] following the correlation given by Eq. (12). The solid line represents a least-squares fit of the experimental data (•) for a semicrystalline sample (60% crystallinity) of PTFEP [7] for eleven gases and small hydrocarbons (He, H_2, Ne, O_2, Ar, CO_2, N_2, CH_4, Kr, Xe, and C_3H_8). Least-squares lines obtained from experimental data [25] for PnBuP, PiBuP, and PsBuP are shown for comparison.

suggested that differences in selectivity may be attributed to the significantly higher main-chain and side-chain flexibility of PnBuP. Following this line of reasoning, comparison of experimental data for PTFEP and for PsBuP (Fig. 4) suggests a comparable state of restricted chain mobility for these two polyphosphazenes.

Representative plots of the average MSD of four CH_4 molecules in both the 150-r.u. amorphous PTFEP cell and the α-orthorhombic supercell at 298 K are shown in Fig. 5. As illustrated, the Einstein diffusion regime [55,59], identified by a region of linearity in the plot of log MSD versus log time, Eq. (7), was observed to begin near 300 ps for both cells.

Diffusion coefficients obtained from the MSD data for seven gases (He, H_2, O_2, CO_2, N_2, CH_4, and Xe) in the two amorphous cells (120- and 150-r.u.) and the α-orthorhombic supercell are plotted against the square of the effective gas diameter in Fig. 6 following the Teplyakov–Meares correlation (Eq. (12)). Experimental (time-lag) data for the semicrystalline samples are also included. The current MD simulations show that, with the exception of He and H_2 as discussed below, gas diffusion coefficients in the two amorphous cells and in the crystalline supercell are comparable to each other and to the experimental data for the semicrystalline samples. These results support the previously mentioned conclusion of Mizoguchi et al. [17] that diffusion is unaffected by crystallinity of PTFEP as illustrated by a plot of CO_2 diffusion coefficients (both simulation and experimental values) against weight fraction crystallinity in Fig. 7. It is noted extrapolation of diffusion coefficients (time-lag data) for CO_2 in PMP against percent crystallinity also resulted in a non-zero value at 100% crystallinity [37,60]; however, diffusion in PMP is not as totally unaffected by crystallinity as it appears to be the case for PTFEP.

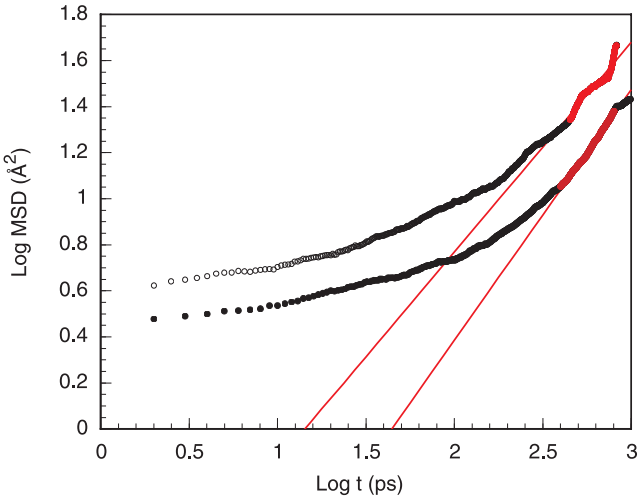

Fig. 5. Representative MSD plot, log MSD versus log t, for methane diffusion (averaged for four methane molecules) in the 150-r.u.amorphous cell (•) and in the α-orthorhombic supercell (○) of PTFEP at 298 K. Lines are fitted to diffusion data in the Einstein region (400–800 ps for the amorphous cell and 450–825 ps for the α-orthorhombic supercell).

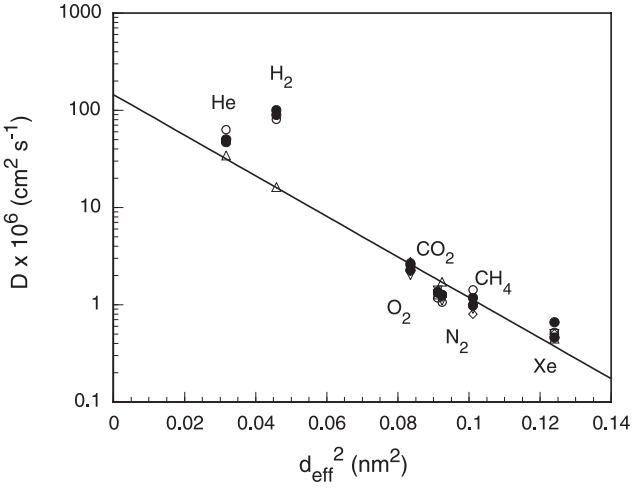

Fig. 6. Plot of both experimental and MD simulation values of diffusion coefficients (D) against the square of the effective gas diameters as tabulated by Teplyakov and Meares [26] following the correlation given by Eq. (12). The solid line represents a least-squares fit of the experimental (time-lag) data (△) for a semicrystalline sample (60% crystallinity) of PTFEP [7] for eleven gases and small hydrocarbons (He, H_2, Ne, O_2, Ar, CO_2, N_2, CH_4, Kr, Xe, and C_3H_8). Additional experimental data points include values [19] for a semicrystalline sample of 31–34% crystallinity (◇) and a sample of 58–65% crystallinity (▽). Simulation results (this study) are shown for both 120- and 150-r.u. amorphous cells (•) and the α-orthorhombic supercell (σ).

In the case of unit cells of PMP, Müller-Plathe [47] had reported that CO_2 diffusion was greater by about 50% parallel to the helix direction than perpendicular to it. In the present study, directional diffusion coefficients were obtained for CO_2 in both the amorphous cell and the

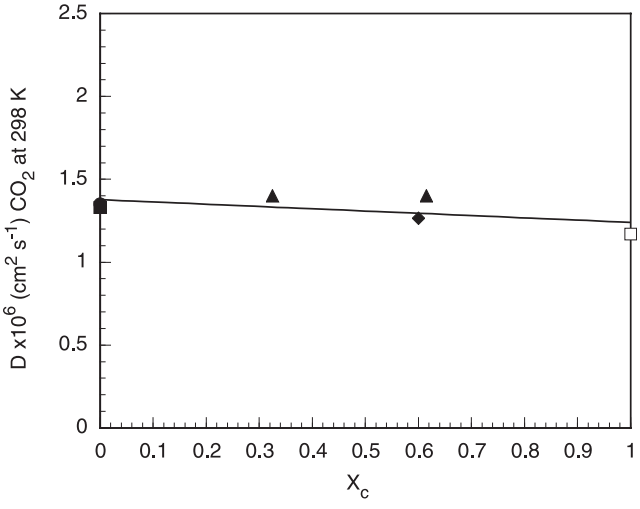

Fig. 7. Plot of experimental and simulation diffusion coefficients of CO_2 against fractional crystallinity (X_c) of PTFEP. (■) Simulation of diffusion in the 120-r.u. amorphous cell (this study); (•) simulation of diffusion in the 150-r.u. amorphous cell (this study); (□) simulation (α-orthorhombic supercell, this study); (▲) experimental (time-lag) data for 31–34% and 58–65% crystallinity [19]; (♦) experimental value for 60% crystallinity [7].

Table 2
Directional diffusion coefficients ($\times 10^7$ cm^2 s^{-1}) obtained for CO_2 in the amorphous cell and α-orthorhombic supercell

	Amorphous	Supercell
D_{xx}	4.3	1.5
D_{yy}	4.8	4.3
D_{zz}	4.3	4.7

crystalline supercell of PTFEP as shown in Table 2. Results indicate that diffusion is isotropic in the amorphous cell as would be expected. In the case of the supercell, CO_2 diffusion, while unrestricted along the chain direction (D_{zz}), is reduced perpendicular to the chain direction (i.e. $(D_{xx}+D_{yy})/2 = 0.29\times10^{-6}$ cm^2 s^{-1}) as in the case of PMP.

It previously noted, simulation values for the self-diffusion coefficients of both He and H_2 are higher than the time-lag data reported by Hirose et al. [7]. Although we have not looked at the simulation of H_2 diffusion in prior work, we have experienced a similar overestimation of the He diffusion coefficient in other polymers including PnBuP and PsBuP, as reported in the prior communication [1]. The problem may be attributed to the use of the non-bonded parameters for He and H_2 contained in the COMPASS force field [3] to model their diffusion as isolated molecules within the rubbery or crystalline phase of a polymer at ambient temperature. It is noted that the L-J parameters in COMPASS were obtained [3] by fitting the condensed-phase properties of the pure gases at their boiling points. The normal boiling points are only 4.2 K for He and 20.4 K for H_2. These boiling temperatures are more than 250 K below the simulation temperature of 298 K. Simulations of the diffusion coefficients for the heavy gases, particularly O_2, N_2, CH_4, and CO_2, have been successful using COMPASS in this and other studies. It may also be noted that while extensive validation of PVT data has been reported for liquid N_2 [3] and for CO_2 [1,3] using COMPASS, it has not been comparably done for He and H_2 at this time.

3.2. Chain flexibility

Plots of main-chain and side chain VACFs (Eq. (9)) are shown in Fig. 8(a) and (b), respectively. For comparison, the main-chain VACF of poly[1-(trimethylsilyl)-1-propyne] (PTMSP), a high-temperature, high-free volume, glassy polymer, is included in Fig. 8(a). Results indicate that mobility of the main chain (Fig. 8(a)) of PTFEP is highly restricted. On the basis of the VACF results, chain flexibility increases in the order PnBuP > PiBuP > PsBuP > PTFEP > PTMSP. There is surprisingly little difference between the main-chain VACFs of amorphous and crystalline PTFEP. By comparison, motions of the trifluoroethoxy side chains of PTFEP are more active for amorphous PTFEP than for the α-orthorhombic supercell as shown in Fig. 8(b). As in the case of the main-chain motions, side-chain mobility is

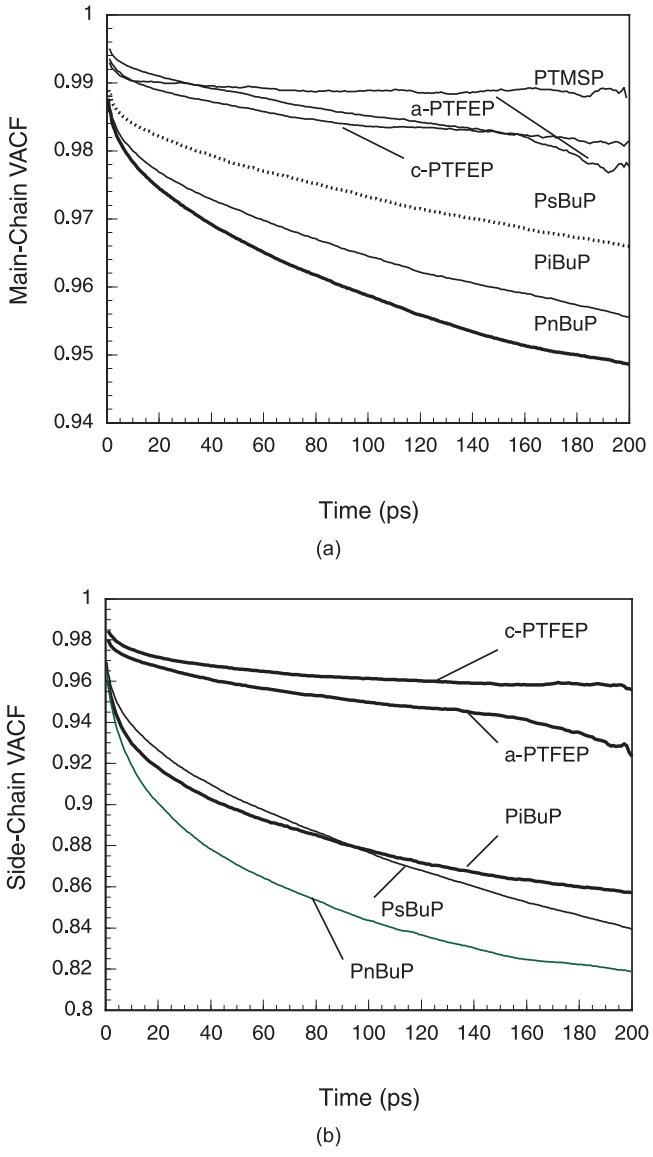

Fig. 8. (a) Plot of the main-chain vectorial autocorrelation function (VACF) for poly[1-(trimethylsilyl)-1-propyne] (PTMSP), PnBuP, PiBuP, PsBuP, and amorphous (150-r.u.) and crystalline (α-orthorhombic) PTFEP. (b) Plot of the side-chain VACF for PnBuP, PiBuP, PsBuP, and amorphous (150-r.u.) and crystalline (α-orthorhombic) PTFEP.

higher for the polybutoxyphosphazenes, particularly in the case of the flexible *n*-butoxy substituent group of PnBuP.

In the case of PTMSP, high diffusivity can be attributed to the extremely high free volume of this polymer as shown in an earlier simulation using a specially parameterized DREIDINGII force field [61]. The static free volume fractions of PnBuP, PiBuP, and PsBuP as determined by the transition-state method of Gusev and Suter [62,63] are comparable to other rubbery polymer near 0.09 while that of PTFEP is actually a little higher at approximately 0.154 (Table 1). In the case of these low-T_g polyphosphazenes, it is reasonable to expect that diffusivity is more strongly related to main-chain and side-chain flexibility in relation to the ability of the chain to create transient regions of free

volume. In the case of the polyphosphazenes, it may be possible to correlate main-chain flexibility with the slope of the Teplyakov–Meares plot of log D versus d_{eff}^2 (Fig. 4). The most flexible main chain of the four polyphosphazenes is PnBuP. PnBuP also has the lowest diffusive selectivity (i.e. the smallest slope). The ordering of main-chain flexibility from VACF given above parallels the decrease in slope (i.e. the loss of diffusive selectivity) in the order PTFEP > PsBuP > PiBuP > PnBuP.

3.3. Gas solubility

Representative low-pressure sorption isotherms obtained from GCMC simulation of three gases (CO_2, CH_4, and He) in amorphous PTFEP (150-r.u. cell) and in the α-orthorhombic PTFEP are shown in Fig. 9(a) and (b), respectively. Solubility coefficients obtained from the isotherms are listed in Table 3. As the data indicate, gas sorption in the crystalline cell is negligible while gas solubilities in the two amorphous cells are nearly an order of magnitude larger than the experimental solubility coefficients reported for the semicrystalline samples [7,19]. The experimental values reported for the semicrystalline samples are effective solubility coefficients obtained from steady-state permeability measurements from the equation

$$S = \frac{P}{D_{\text{TL}}} \tag{13}$$

where P is the permeability coefficient and D_{TL} is the time-lag diffusion coefficient [64,65]. Adjusting for the crystalline content by means of the two-phase approximation represented by Eq. (6) brings the solubility data of the semicrystalline samples closer to that of the amorphous cell simulation results; however, the 'effective' amorphous-phase solubility coefficients of the semicrystalline samples are still a factor of four or five smaller than those obtained from GCMC simulation of the 150-r.u. amorphous cell as shown by data included in Table 4. As mentioned earlier, GCMC simulation of an amorphous cell of PsBuP reported in the prior communication [1] also yielded solubility coefficients that are five to six times larger that those reported from permeability measurements of uncharacterized samples [25]. In contrast, there was very good agreement between experimental and amorphous simulation data for PnBuP which is believed to be a totally amorphous polymer. In the previous communication [1], the anomalous solubility results for PsBuP were tentatively attributed to an effect of a crystalline or a mesomorphic structure in the experimental sample. Mesophase formation is less likely [66] for longer-chain alkoxy-substituted polyphosphazenes such as PnBuP and, therefore, the experimental data should be that of a totally amorphous state in that case.

Experimental values of the solubility coefficients, Eq. (13), and those obtained from GCMC simulation of amorphous PTFEP cells for the seven gases are plotted against the Lennard-Jones potential-well depth parameter, ε/k, in Fig. 10. As shown, both the experimental and simulated solubility coefficients of each gas closely follow the Teplyakov and Meares correlation given by Eq. (2) with sole exception of CO_2 which falls significantly above the linear relationship. As mentioned earlier, ab initio and molecular simulation studies in our laboratory have assigned the high solubility of CO_2 in PTFEP to a weak quadrupole–dipole interaction between CO_2 and the electron-withdrawing trifluoroethoxy groups of PTFEP [35]. The agreement between the experimental study of Hirose et al. [7] and Starannikova et al. [19] and the GCMC simulation results in regard to elevated CO_2 solubility demonstrates the ability of the class II COMPASS force field to reproduce even weak specific interactions through parameterization using condensed-phase data. In the case of specific interactions, Eq. (2) is inadequate but can be

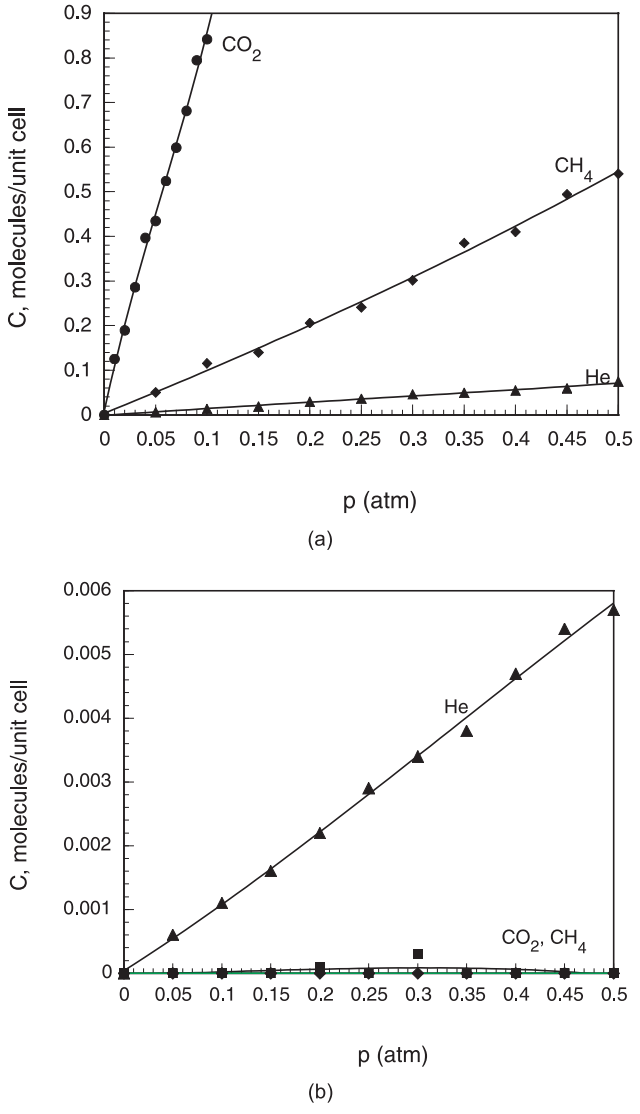

Fig. 9. (a) Representative sorption isotherms for He, CH_4, and CO_2 in the (150-r.u.) amorphous cell of PTFEP. (b) Representative sorption isotherms for He, CH_4, and CO_2 in the α-orthorhombic supercell.

Table 3
Gas solubility coefficients in PTFEP at 298 K

S ($\times 10^3$ cm^3 (STP) cm^{-3} cm Hg^{-1})						
Gas	ε/k (K)[a]	Simulation (GCMC)			Experiment	
		Amorphous (120-r.u.)	Amorphous (150 -r.u.)	Crystalline supercell	Sample 1[b] (X_a=0.4)[d]	Sample 2[c] (X_a=0.7)[d]
He	9.5	2.45	2.82	0.19	0.28	NA
H_2	62.2	3.31	4.89	0.005	0.4	NA
N_2	83.0	10.1	12.2	0.002	0.9	2.6
O_2	112.7	12.6	15.2	<0.001	1.3	3.3
CH_4	154.7	16.0	18.7	<0.001	1.7	4.5
CO_2	213.4	138.2	180.3	<0.001	15.5	26.4
Xe	232.9	50.3	60.9	<0.001	5.2	9.2

[a] Values taken from Teplyakov and Meares [26].
[b] Effective solubility coefficients, Eq. (13), reported by Hirose et al. [7].
[c] Effective solubility coefficients, Eq. (13), reported by Starannikova et al. [19].
[d] X_a, amorphous weight fraction of the semicrystalline samples.

modified by introducing a Flory interaction parameter as described in the Section 3.4.

As mentioned earlier, the Widom method had been used by Müller-Plathe [47] and by Zanuy et al. [50] for the simulation of gas solubility in poly(4-methyl-1-pentene) (PMP). For comparison, the Widom method has been used to determine gas solubility in the amorphous (150-r.u.) cell as well as a unit cell, two unit cells, and in the α-orthorhombic supercell. Results are summarized in Table 5. As shown in Fig. 10, there is good agreement between solubility coefficients obtained from both the GCMC and Widom methods for the amorphous cells but solubility is still negligible in the crystalline cells for gases larger than He.

3.4. Modification of the Teplyakov correlation

As a simple approach to incorporate an interaction term into the Teplyakov–Meares correlation (Eq. (2)), we borrow from the early work of Michaels and Bixler [44]. In their classical paper on the solubility of gases in polyethylene, they obtained an approximate expression for the chemical potential (units of kJ mol^{-1}) of an ideal gas as

$$\mu_{dg} = 0.0654\left(\frac{\varepsilon}{k}\right) - 24.97 \tag{14}$$

In the case of low gas solubility in a high-molecular-weight rubbery polymer, the Flory–Huggins expression [67] for the chemical potential of the dissolved gas reduces to

$$\mu_{dg} = RT(\ln \phi_1 + 1 + \chi) \tag{15}$$

where ϕ_1 is the volume fraction of the dissolved gas and χ is the (Flory) interaction parameter. The relationship between the solubility coefficient and ϕ_1 at 1 atm is

$$S = \frac{24,400\phi_1}{\bar{V}_1} \tag{16}$$

where $\bar{V}_1$ is the partial molar liquid volume of the dissolved gas [44]. Substitution of Eq. (16) rearranged for ϕ_1 into Eq. (15) gives

$$\mu_{dg} = RT[\ln(S\bar{V}_1) - \ln 24,400 + 1 + \chi]$$
$$= RT[(S\bar{V}_1) - 9.102 + \chi] \tag{17}$$

Equating chemical potentials, Eqs. (14) and (17), and rearranging for S gives (at 298 K)

Table 4
Gas solubility in amorphous part of PTFEP samples

S ($\times 10^3$ cm^3 (STP) cm^{-3} cm Hg^{-1})			
Gas	Simulation of amorphous cells[a]	Amorphous contribution[b] in sample 1[c] (X_a=0.4)	Amorphous contribution[b] in sample 2[d] (X_a=0.7)
He	2.82	0.7	NA
H_2	4.89	1.0	NA
N_2	12.2	2.25	3.71
O_2	15.2	3.25	4.71
CH_4	18.7	4.25	6.43
CO_2	180.3	38.8	37.7
Xe	60.9	13.0	13.1

[a] Solubility coefficients obtained from GCMC simulations of the 150-r.u. amorphous cell.
[b] Calculated from the two-phase model given by Eq. (6), using the reported the amorphous weight fractions, X_a, of the semicrystalline samples.
[c] Data from Hirose et al. [7,25].
[d] Data from Starannikova et al. [19].

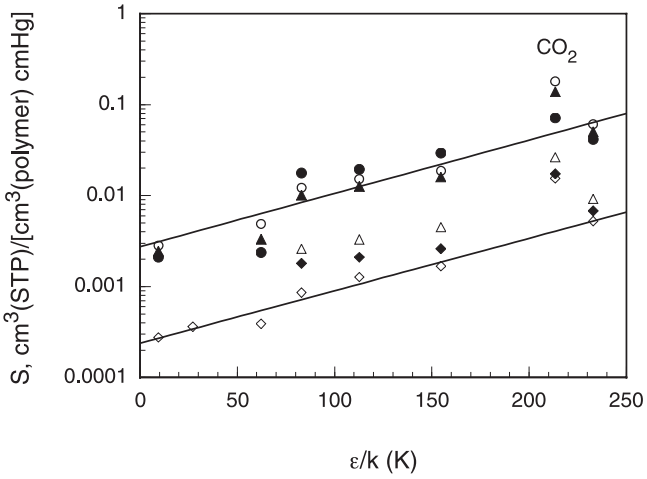

Fig. 10. Semilogarithmic plot of gas solubility coefficients for eight gases in PTFEP versus Lennard-Jones well-depth parameter, ε/k, following the correlation given by Eq. (2). Experimental data: (◇) 60% crystalline [7]; (△) 31–34% crystalline [19]; (♦) 58–65% crystallinity. Simulation results: (•) 150-r.u. amorphous cell, Widom method; (○) 150-r.u. amorphous cell, GCMC method; (▲) 120-r.u. amorphous cell, GCMC method. Upper line represents least-squares fit of GCMC data (○) of 150-r.u., amorphous cell; lower line represents least-squares fit of experimental data (ε) of Hirose et al. [7] for PTFEP (60% crystallinity). In both cases, CO_2 is excluded from least-squares fit of data.

$$\ln S = -\ln \bar{V}_1 + 9.102 - \chi + \left(\frac{0.0654(\varepsilon/k) - 24.97}{0.0083144(298)}\right) = -\ln \bar{V}_1 - 0.976 - \chi + 0.0260\left(\frac{\varepsilon}{k}\right) \quad (18)$$

Eq. (18) can be rearranged in the form

$$\ln S = a\left(\frac{\varepsilon}{k}\right) - \ln \bar{V}_1 - \chi - b \quad (19)$$

With the assumption that both χ and $\bar{V}_1$ are both proportional to ε/k [44], Eq. (19) takes the form of the Teplyakov–Meares correlation given by Eq. (2). In the case of specific interactions such as the quadrupole–dipole interaction of CO_2 with the trifluoroethoxy group of PTFEP, the interaction parameter χ needs to remain an explicit part of the equation as indicated by the failure of the Teplyakov–Meares correlation for CO_2 as shown in Fig. 10.

Table 5
Solubility coefficients obtained by Widom test-particle methods at 298 K

Gas	Amorphous (150-r.u.)	Unit cell	Two unit cells	Supercell
He	2.37	0.0216	0.0165	0.00134
H_2	2.10	0.0211	0.0208	0.00473
N_2	17.7	0.00734	0.00851	<0.001
O_2	19.4	0.00728	0.0200	<0.001
CH_4	29.4	0.00216	0.0302	<0.001
CO_2	71.4	0.00507	<0.001	<0.001
Xe	41.4	0.00127	<0.001	<0.001

$\times 10^3$ cm^3 (STP)/(cm^3 polymer-cm Hg).

In this case, Eq. (19) can be expressed in the form

$$\ln S = 0.026\left(\frac{\varepsilon}{k}\right) - \chi - K \quad (20)$$

or

$$\log S = 0.011\left(\frac{\varepsilon}{k}\right) - \chi' - K' \quad (21)$$

where K is a constant that incorporates $\bar{V}_1$. Although experimental values of partial molar volumes for gases dissolved in a specific polymer are not generally available, the general success of the Teplyakov equation, Eq. (2), suggests that incorporation of $\bar{V}_1$ into the constant K may be a reasonable approximation here. In order to use Eq. (20) or (21), values of χ for each gas in PTFEP are needed. These values can be approximated from the experimental solubility and use of the Flory–Huggins equation for an ideal gas at 1 atm pressure and low gas solubility as [68]

$$\chi = \ln\left(\frac{p_1}{p_1^0}\right) - \ln \phi_1 - 1 \quad (22)$$

where p_1 is the gas partial pressure (1.0 atm in this case) and p_1^0 is the saturated vapor pressure of the gas at room temperature obtained by extrapolating log p_1^0 versus $1/T$ [69]. Eq. (16) was used to calculate ϕ_1 from the effective solubility coefficients reported by Hirose et al. [7]. All values of S, p_1^0, ϕ_1, and χ are tabulated in Table 6. Experimental and simulation solubility coefficients are plotted against $0.0026(\varepsilon/k) - \chi$ in Fig. 11. As shown, solubility data for CO_2 is now reasonably represented by the modified correlation given by Eq. (20).

4. Discussion and conclusions

Molecular dynamics and Monte Carlo simulation have shown that PTFEP in its α-orthorhombic crystalline form permits free diffusion of gases as large as Xe (effective diameter of 3.52 Å) but does not absorb gases larger than He (1.78 Å). This is in contrast to most crystalline polymers for which neither gas diffusion or solubility occurs in the densely packed crystalline domains. PTFEP also differs from PMP and the δ_e crystalline form of sPS that permit both sorption and diffusion of gases. ^{125}Xe NMR measurements of Xe sorbed in the δ_e form of PMP [70] reveals a cavity size of approximately 4.5 Å through which small gas molecules can pass but molecules with kinetic diameters greater than 4.5 Å (e.g. C_3H_8 and t-C_4H_{10}) can not. It is noted that in contrast to permeation behavior of the δ_e crystalline form of PMP, noble gases (i.e. He, Ne, and Ar) have only limited solubility but can diffuse in the β crystalline form of PMP due to its smaller cavity sizes [42]. The experimental d-spacing between PTFEP backbone chains has been reported to be only 4.31 Å [71]. This suggests a smaller cavity size (Fig. 3) consistent with the very limited gas solubility of the orthorhombic α-form.

Table 6
Values of the gas interaction parameter in PTFEP

Gas	(ε/k)[a] (K)	(p_1^0)[b] (atm)	(S)[c] $\times 10^3$ (STP) $cm^3\ cm^{-3}$ (polymer) atm^{-1}	ϕ_1	χ	0.0260 (ε/k)-χ
He	9.5	2500	21.3	2.6×10^{-5}	1.72	−1.473
H_2	62.2	1250	30.4	6.8×10^{-5}	1.47	0.1472
N_2	83.0	1000	68.4	1.5×10^{-4}	0.88	1.278
O_2	112.7	700	98.8	2.2×10^{-4}	0.87	2.060
CH_4	154.7	370	129.2	2.9×10^{-4}	1.24	2.782
CO_2	213.4	63.5	1178	3.3×10^{-3}	0.56	4.988
Xe	232.9	78.1	395.2	8.8×10^{-4}	1.68	4.375

[a] Values taken from Teplyakov and Meares [26].
[b] Values taken from Refs. [68,69].
[c] Data of Hirose et al. [7].

The greater sensitivity of sorption to void or free volume distribution compared to diffusion can be inferred from the MD studies of Wagner and co-workers [72,73] who investigated the effect of periodic cell size on the MD simulation of diffusion and sorption (using the Widom particle insertion method [48,49]). They showed that solubility coefficients obtained for larger gases such as CO_2 and CH_4 in smaller cells are anomalously low while cell size has little effect of the values of the self-diffusion coefficients of these gases. These results suggest that small boxes are unable to generate sufficiently large cavity sizes to accommodate sorption of the larger molecules [72]. They noted that the diameter of the largest spherical cavity increases from approximately 3.5–4.5 Å when the cell size doubles from 20 to 40 Å. The absence of cavities larger than 3.5 Å limits the solubility of the larger gas molecules such as CH_4 and CO_2.

The results of GCMC simulation of gas solubility in the amorphous phase suggests that the presence of crystallites in semicrystalline samples may significantly reduce gas solubility in the amorphous region. Recently, a similar argument been made for polyethylene which was the model for gas sorption in semicrystalline polymers selected by Michaels and Bixler in their classic paper [44]. Recently, Budzien et al. [46] have concluded from extrapolation of gas solubility data in alkanes that solubility in the amorphous phase of polyethylene may be higher than the simple two-phase model represented by Eq. (6) would predict. In their paper, Budzien et al. addressed the simulation data for gas solubility in polyethylene reported by van der Vegt et al. [74]. Solubilities obtained using the Widom method were consistently three to six times larger than 'experimental' values for 100% amorphous polyethylene calculated from Eq. (6). Results reported in the present simulation study suggest similarly large gas solubilities in amorphous PTFEP (Table 4) as also reported for PsBuP in the prior publication [1]. The reasons for the effect of crystallites on gas solubility in the amorphous phase are not known at this time. In terms of chain immobilization, diffusion results for PTFEP would suggest that tortuosity and chain immobilization factors, Eq. (5), are negligible for this polymer. If solubility is affected by crystallites present in semicrystalline PTFEP it may be through reduction in the free volume distribution of the amorphous phase. Positron lifetime studies, as well as

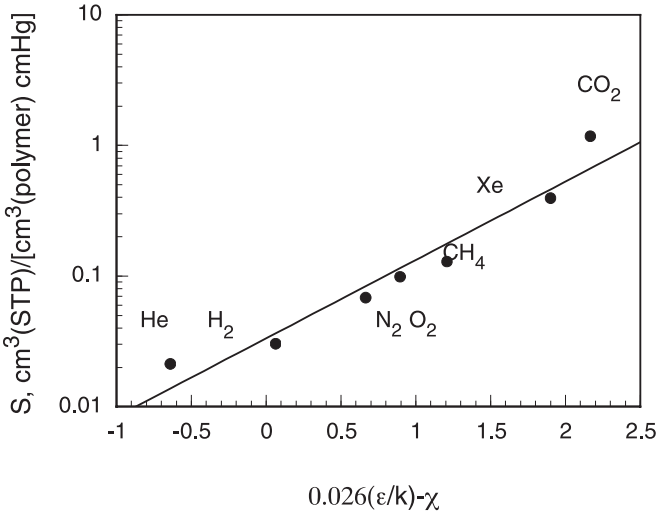

Fig. 11. Semilogarithmic plot of gas solubility coefficients for seven gases in PTFEP versus the $0.026(\varepsilon/k)-\chi$, following the correlation given by Eq. (20). Line represents a least-squares fit of all data [7], including CO_2 ($R^2=0.9381$).

gravimetric solubility measurements of amorphous and crystalline PTFEP sample, would be helpful to clarify these issues.

Acknowledgements

Major support from the Ohio Board of Regents (Investment Fund) for computer facilities and software used in these studies is greatly appreciated. The current study is based partially upon work supported by the National Science Foundation under Grant No. 9810320. We particularly want to express our gratitude to Dr Pengyu Ren, Department of Biochemistry and Molecular Biophysics of the Washington University Medical School, for his initial simulation studies of polyphosphazenes and for many helpful discussions during the preparation of the current manuscript.

References

[1] Fried JR, Ren P. Comput Theor Polym Sci 2000;10:447–63.
[2] Sun H. J Phys Chem B 1998;102:7338–64.
[3] Yang J, Ren Y, Tian An-m, Sun H. J Phys Chem B 2000;104:4951–7.
[4] McQuaid MJ, Sun H, Rigby D. J Comput Chem 2003;25:61–71.
[5] Sun H, Ren P, Fried JR. Comput Theor Polym Sci 1998;8:229–46.
[6] Fried JR, Ren P. Comput Theor Polym Sci 1999;9:111–6.
[7] Hirose T, Kamiya Y, Mizoguchi K. J Appl Polym Sci 1989;38: 809–20.
[8] Singler RE, Schneider NS, Hagnauer GL. Polym Eng Sci 1975;15: 321–38.
[9] Schneider NS, Desper CR, Singler RE. J Appl Polym Sci 1976;20: 3087–31103.
[10] Young SG, Kojima M, Magill JH, Lin FT. Polymer 1992;33:3215–25.
[11] Gleria M, Bertani R, Jaeger RD. J Inorg Organomet Polym 2004;14: 1–28.
[12] Kojima M, Magill JH. Polym Commun 1983;24:329–31.
[13] Kojima M, Magill JH. Polym Commun 1984;25:273–5.
[14] Kojima M, Kluge W, Magill JH. Macromolecules 1984;17:1421–5.
[15] Kojima M, Magill JH. Polymer 1985;26:1971–8.
[16] Ciora RJ, Magill JH. Macromolecules 1990;23:2350–9.
[17] Mizoguchi K, Kamiya Y, Hirose T. J Polym Sci Part B: Polym Phys 1991;29:695–703.
[18] Allcock HR, Nelson CJ, Coggio WD, Manners I, Koros WJ, Walker DRB, et al. Macromolecules 1993;26:1493–502.
[19] Starannikova LE, Tur DR, Teplyakov VV, Platé NA. Polym Sci 1994; 36:1610–5.
[20] Antipov EM, Kulichikhin VG, Golova LK, Kruchinin NP, Tur DR, Platé NA. Polym Sci USSR 1990;32:108–15.
[21] Alexander MN, Desper CR, Sagalyn PL, Schneider NS. Macromolecules 1977;10:721–3.
[22] Ferrar WT, Marshall AS, Whitefield J. Macromolecules 1987;20: 317–22.
[23] Fried JR, Hu N. Submitted for publication.
[24] Toi K, Morel G, Paul DR. J Appl Polym Sci 1982;27:1997–2005.
[25] Hirose T, Mizoguchi K. J Appl Polym Sci 1991;43:891–900.
[26] Teplyakov V, Meares P. Gas Sep Purif 1990;4:66–74.
[27] Stern SA. J Membr Sci 1994;94:1–65.
[28] Shah VM, Hardy BJ, Stern SA. J Polym Sci Part B: Polym Phys 1986; 24:2033–47.
[29] Stern SA, Shah VM, Hardy BJ. J Polym Sci Part B: Polym Phys 1987; 25:1263–98.
[30] Hellums MW, Koros WJ, Husk GR, Paul DR. J Membr Sci 1989;46: 93–112.
[31] El-Hibri MJ, Paul DR. J Appl Polym Sci 1986;31:2533–60.
[32] Chiou JS, Paul DR. J Appl Polym Sci 1986;32:4793–814.
[33] Masuda T, Iguchi Y, Tang B-Z, Higashimura T. Polymer 1988;29: 2041–9.
[34] Yampol'skii YP, Bespalova NB, Finkel'shtein ES, Bondar VI, Popov AV. Macromolecules 1994;27:2872–8.
[35] Fried JR, Hu N. Polymer 2003;44:4363–72.
[36] Puleo AC, Paul DR, Wong PK. Polymer 1989;30:1357–66.
[37] Tsujita Y. Chin J Polym Sci 2000;18:301–7.
[38] Kusanagi H, Takase M, Chatani Y, Tadokoro H. J Polym Sci Part B: Polym Phys 1978;16:131–42.
[39] Manfredi C, Del Noble MA, Mensitieri G, Guerra G, Rapacciuolo M. J Polym Sci Part B: Polym Phys 1997;35:133–40.
[40] Guadagno L, Baldi P, Vittoria V, Guerra G. Macromol Chem Phys 1998;199:2671–5.
[41] Yamamoto Y, Kishi M, Amutharani D, Sivakumar M, Tsujita Y, Yoshimizu H. Polym J 2003;35:465–9.
[42] Tamai Y, Fukuda M. Polymer 2003;44:3279–89.
[43] Paul DR. Transport properties of polymers. In: Tess RW, Poehlein GW, editors. Appl Polym Sci. Washington, DC: ACS; 1985. p. 253–75.
[44] Michaels AS, Bixler HJ. J Polym Sci 1961;50:393–412.
[45] Mogri Z, Paul DR. Polymer 2001;42:2531–42.
[46] Budzien JL, MCoy JD, Weinkauf DH, LaViolette RA, Peterson ES. Macromolecules 1998;31:3368–71.
[47] Müller-Plathe F. J Chem Phys 1995;103:4346–51.
[48] Widom B. J Phys Chem 1982;86:869–72.
[49] Widom B. J Chem Phys 1963;39:2808–12.
[50] Zanuy D, Aleman C, Munoz-Guerra S. J Polym Sci Part B: Polym Phys 2002;40:2037–49.
[51] Hu N. PhD Dissertation, University of Cincinnati; 2003.
[52] Andrea TA, Swope WC, Andersen HC. J Chem Phys 1983;79: 4576–84.
[53] Berendsen HJC, Potsma JPM, van Gunsteren WF, DiNola A, Haak JR. J Chem Phys 1984;81:3684–90.
[54] Trohalaki S, Kloczkowaski A, Mark JE, Rigby D, Roe RJ. Estimation of diffusion coefficients for small molecular penetrants in amorphous polyethylene. In: Roe RJ, editor. Computer simulation of polymers. Englewood Cliffs, NJ: Prentice Hall; 1991. p. 220–32.
[55] Müller-Plathe F. Acta Polym 1994;45:259–93.
[56] Fan CF, Cagin T, Shi W, Smith KA. Macromol Theory Simul 1997;6: 83–102.
[57] Metropolis N, Rosenbluth AW, Rosenbluth MN, Teller AH, Teller E. J Chem Phys 1953;21:1087–92.
[58] Teplyakov VV, Durgar'yan SG. Polym Sci USSR 1984;10:2415–21.
[59] Gusev AA, Muller-Plathe F, van Gunsteren WF, Suter UW. Adv Polym Sci 1994;116:207–47.
[60] Yoshimizu H, Fukatsu H, Suzuki T, Tsujita Y, Kinoshita T. Polym J 1998;30:981–4.
[61] Fried JR, Goyal DK. J Polym Sci Part B: Polym Phys 1998;36: 519–36.
[62] Gusev AA, Suter UW. J Chem Phys 1993;99:2228–34.
[63] Gusev AA, Arizzi S, Suter UW, Moll DJ. J Chem Phys 1993;99: 2221–7.
[64] Crank J, Parks GS. Diffusion in polymers. London: Academic Press; 1968.
[65] Frisch HL. J Phys Chem 1957;61:93–5.
[66] Tur DR, Provotorova NP, Vinogradova SV, Bakhmutov VI, Galakhov MV, Zhukov VP, et al. Makromol Chem 1991;192: 1905–19.
[67] Flory PJ. Principles of polymer chemistry. Ithaca: Cornell University Press; 1953.
[68] van Amerongen GJ. J Polym Sci 1950;5:307–32.

[69] Hildebrand JH. Solubility in non-electrolytes. New York: Reinhold; 1936.
[70] Suzuki T, Tanaka T, Nakajima M, Yoshimizu H, Tsujita Y. Polym J 2002;34:891–6.
[71] Nakamura H, Masuko T, Kojima M, Magill JH. Macromol Chem Phys 1999;200:2519–24.
[72] Cuthbert TR, Wagner NJ, Paulaitis ME. Macromolecules 1997;30: 3058–65.
[73] Cuthbert TR, Wagner NJ, Paulaitis ME, Murgia G, D'Aguanno B. Macromolecules 1999;32:5017–28.
[74] van der Vegt NF. J Chem Phys 1996;105:8849–57.
[75] Gusev A, Suter UW. Comput Aided Mater Des 1993;1:63–73.